This project has received funding from the European Union's Seventh Programme for research, technological development and demonstration under grant agreement No [308417]".

New Directions in Seismic Hazard Assessment through Focused Earth Observation in the Marmara Supersite

Grant Agreement Number: 308417
co-funded by the European Commission within the Seventh Framework Programme
THEME [ENV.2012.6.4-2]
[Long-term monitoring experiment in geologically active regions of Europe prone to natural hazards: the Supersite concept]

D4.2 Report on the analysis of the response of the near surface geology on earthquake ground motion

Project Start Date	1 November 2012
Project Duration	36 months
Project Coordinator /Organization	Nurcan Meral Özel / KOERI
Work Package Number	4
Deliverable Name/ Number	2
Due Date Of Deliverable	30 April 2016
Actual Submission Date	15 May 2016
Organization/Author (s)	GFZ, Stefano Parolai, Bojana Petrovic

Dissemination Level		
PU	Public	
PP	Restricted to other programme participants (including the Commission)	
RE	Restricted to a group specified by the consortium (including the Commission)	
CO	Confidential, only for members of the consortium (including the Commission)	

TABLE OF CONTENTS

1 INTRODUCTION

Reliable predictions of ground-motion that may arise from future earthquakes can only be obtained by a combination of realistic source, wave propagation and site-response models. Additional information may be obtained from downhole arrays with regards to in-situ surface and laboratory geotechnical investigation techniques, since recordings from these are an useful and important tool for improving our understanding of in-situ soil behavior, including insights into the wave propagation through the shallow geological layers (when deconvolution interferometry is applied). Such information provide critical constraints for both the interpretation methods of surface observations as well as about the real material behavior and overall site response over a wide range of loading conditions (Assimaki et al., 2008). Hence, downhole arrays installed in seismically active areas make it possible to improve our understanding of in-situ soil behavior, to assess modeling and parametric uncertainties associated with employed methodologies for strong-motion site-response analysis, and for shallow geological investigations.

Furthermore, buildings of different construction types and hence with disparate dynamic properties, respond differently to seismic wave excitation. It is also not only the material and structure of a building, but also the soil on which the building is constructed that has an influence on its response to ground motion, while in turn the building's vibrations influence the ground motion.

Hence, information about the dynamic properties of buildings (obtained from vertical arrays of sensors installed at different levels of a structure), the characteristics of the soil (estimated by the analysis of borehole data) and the soil-structure (soil-building) interaction are required to better improve seismic risk assessments. In particular, determining the different contributions to the wavefield recorded at different depths (in the borehole) are necessary to correctly carry out studies dealing with seismic source parameters estimation and wave propagation through the upper-most layers of the earth.

In the past, deconvolution interferometry has been applied separately to recordings of sensors installed in buildings to study wave propagation through the structure arising from earthquakes, synthetic sources and ambient vibration (e.g., Picozzi et al., 2009, Newton and Snieder, 2012, Rahmani and Todorovska, 2013, Nakata et al., 2013, 2015, Nakata and Snieder, 2014, Cheng et al., 2015) and to earthquake recordings of borehole sensors (e.g., Mehta et al., 2007a, 2007b, Parolai ei al., 2009, 2010, 2012, 2013 Oth et al., 2011) to investigate the wave propagation in shallow geological layers. However, the joint application to systems including both soil and structure has so far received limited attention. As a matter of fact, waves traveling from the soil to the building and the wavefield radiated back from the building to the soil can only be analyzed if the recordings of sensors installed in both, i.e., in a borehole and in nearby buildings, are available and jointly analyzed.

2 METHODOLOGY

2.1 DECONVOLUTION

The deconvolution interferometry method is a tool that allows the investigation of wave propagation both through buildings and soil. It is based on the deconvolution of the signal $u(t)$ recorded at a generic location by $u_{ref}(t)$, which is the signal recorded at a reference location. In the frequency domain, the deconvolution is defined as (Snieder and Safak, 2006)

$$D(\omega) = \frac{u(\omega)u^*_{ref}(\omega)}{|u_{ref}(\omega)|^2 + \epsilon}$$

where $\omega = 2\pi f$ is the angular frequency and ϵ is a regularization parameter that controls the degree of filtering used to stabilize the deconvolution.

2.2 CONSTRAINED DECONVOLUTION

The recordings at the base of a borehole are contaminated with signals reflected from the free surface, the so-called downgoing waves. Therefore, there is a need to mitigate this effect in order to obtain the seismic input motion. The seismic input motion $I(t)$ at the base of an instrumented borehole can be determined using the recordings of only a pair of sensors (one at the borehole surface $S(t)$ and one at the base $B(t)$) and applying a constrained deconvolution approach (Bindi et al., 2010). Knowledge of the soil profile is not required for this proceedure. The determination of the propagator from the surface to the base of the borehole in the Fourier domain is performed by the deconvolution of the signal $S(t)$ recorded at the surface from the downhole recording $B(t)$ as follows:

$$\frac{\hat{B}}{\hat{S}} = \frac{\hat{I} + \hat{I}\hat{P}_T}{2\hat{I}\hat{P}_U} = \frac{1 + \hat{P}_T}{2\hat{P}_U} = \frac{1}{2\hat{P}_U} + \frac{\hat{P}_D}{2}$$

where P_U and P_D are the propagators for waves traveling from the base to the surface and vice versa, respectively, and P_T is the total propagator. The ^ indicates the Fourier transforms.

An iterative regularization algorithm that allows us to constrain the solution to be positively defined and to have a finite time duration (the time frame outside of which the propagator is set to zero is selected visually), is applied to stabilize the bottom-to-surface spectral ratio. The modified Landweber method (e.g., Bertero and Boccacci, 1998), including a priori constraints on the solution (Bertero et al., 1997), and defined as

$$f_{n+1} = P_C[f_n + \alpha S^T * (B - S * f_n)]$$

is used. P_C denotes the convex projection onto the closed and convex set C, n is the number of completed iterations, f_n is the regularized solution at iteration n, and α is a relaxation parameter.

2.3 JOINT DECONVOLUTION

The joint deconvolution is based on the regularized Tikhonov deconvolution (Mehta et al., 2007a, 2007b, Parolai et al., 2009)

$$D(\omega) = \frac{u(\omega)u^*_{ref}(\omega)}{|u_{ref}(\omega)|^2 + \varepsilon}$$

and is applied to borehole and building data jointly.

The estimation of the wavefield radiated back to the soil is based on 1) the detailed identification of the peaks of the deconvolved wavefield, 2) the estimation of the real input and 3) the estimation of the part of the wavefield describing the propagation from the building to the ground (Petrovic and Parolai, 2016).
Within the framework of this project, the methodology was developed, tested and first applied to another vertical array installation (in Bishkek, Kyrgyzstan) where more data were available (Petrovic and Parolai, 2016). With this methodology, the approach of Bindi et al. (2010) described in 2.2 is extended to account for and allow the separation in the wavefield of the contribution due to the energy radiated to the ground by the building. For example, if the building is considered as an extra layer above the ground, the deconvolution of the recording in the borehole x(t) with respect to the one at the top of the building y(t) would have the form:

$$\frac{x(\omega)}{y(\omega)} = \underbrace{\frac{1}{2(1+r)}e^{-i2\pi f\left(\frac{-\tau_1}{Q_1}-\frac{\tau_2}{Q_2}\right)}}_{(a)} + \underbrace{\frac{r}{2(1+r)}e^{-i2\pi f\left(\frac{\tau_1}{Q_1}-\frac{\tau_2}{Q_2}\right)}}_{(b)} + \underbrace{\frac{r}{2(1+r)}e^{-i2\pi f\left(\frac{\tau_2}{Q_2}-\frac{\tau_1}{Q_1}\right)}}_{(c)}$$

$$\Big| + \underbrace{0.5(1-r)e^{-i2\pi f\left(\frac{\tau_1}{Q_1}+\frac{\tau_2}{Q_2}\right)}}_{(d)} + \underbrace{\frac{r^2}{2(1+r)}e^{-i2\pi f\left(\frac{\tau_1}{Q_1}+\frac{\tau_2}{Q_2}\right)}}_{(e)}$$

The approach that we have developed allows us to solve this problem in an empirical way, even in more complicated media where all the parameters for defining an analytical solutions are not available.

3 TEST SITES

3.1 THE GAZIKÖY VERTICAL ARRAY

The installation of a multi-parameter borehole system in Gaziköy, Turkey (location shown in Fig. 1), next to the main Marmara fault, consists of a tiltmeter (at -145 m), two broad-band seismometers (-143.6 m and 0 m) and two strong-motion accelerometers (at -142.3 m and 0 m).

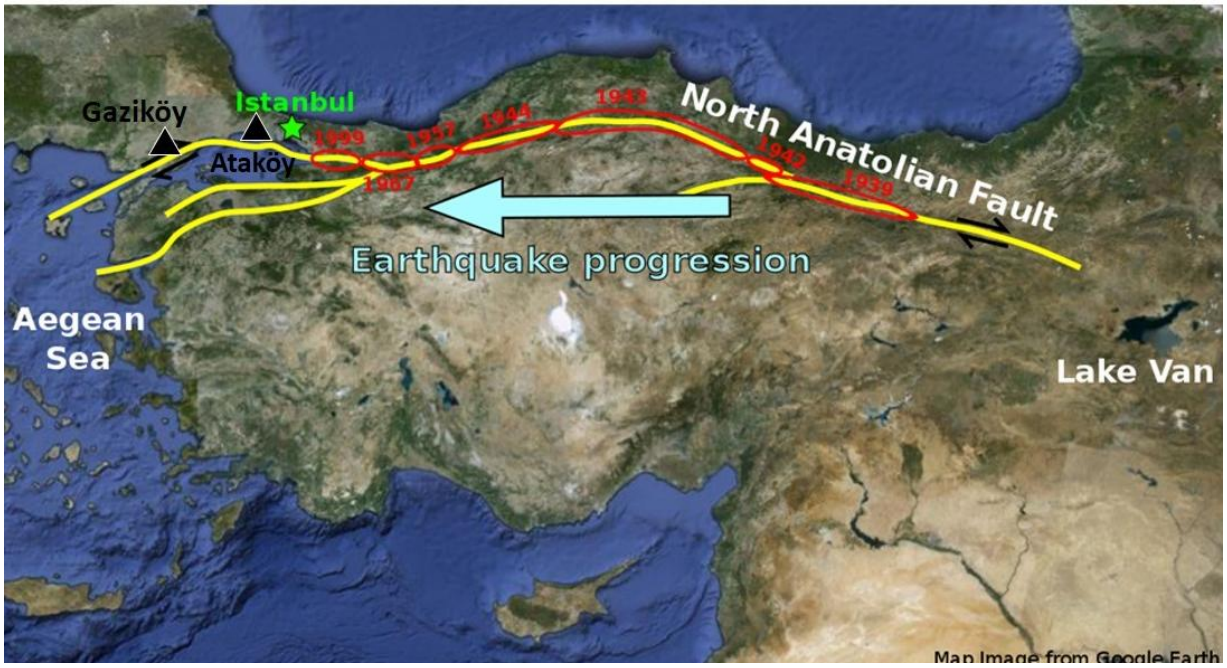

Figure 1. Location of the borehole installations close to the main Marmara fault in Gaziköy, and the one in Ataköy, Turkey (redrawn after https://thepalebluedot.co.uk/tag/istanbul/).

3.2 THE ATAKÖY VERTICAL ARRAY

The data used in the studies was acquired from a downhole array and building (B22) pair (the distance apart being around 30m) located in the Ataköy district, Istanbul, Turkey (location shown in Fig. 1). The stratigraphy at the test site and the results of SPT tests, as well as the velocity profile of the soil, are shown in Fig. 2 (right) (Parolai et al., 2009, 2010, 2012).

B22 is a residential building constructed in the early 1990's by tunnel formwork (Fig. 2 left and center). It is 16 stories high (about 45 m), including one basement floor. The standard floor height is 2.80 m. The building is symmetrical plan view in both perpendicular directions. The plan dimensions are approximately 23.10 m x 23.90 m. The interior walls are 20 cm thick reinforced concrete. The exterior walls were formed by precast panels. Four apartments are located at each floor (two at each side of the common corridor that is parallel to the x-direction), with the same size and the same floor layout. The building has two elevators, one on each side of the corridor, an interior reinforced concrete staircase and an exterior steel fire escape staircase.

The B22 building is equipped with 14 SOSEWIN (Self-organizing Seismic Early Warning Information Network) stations installed on 7 floors at two locations within the building (center of the building and fire escape staircase) as shown in Fig. 2 (left and center). The data is transmitted in real-time. The downhole array (Parolai et al., 2009, 2010, 2012, Bindi et al., 2010, Dikmen et al., 2015, 2016) consists of three shallow borehole accelerometers (SBEPI) at 25m, 50m and 70m depth and a

downhole borehole accelerometer (ES-DH) at 140 m depth. An accelerometer is installed also at 0m. The accelerometer at 70m (SBEPI) depth, due to an electronic malfunction, did not acquire usable data during some events. Hence, it is left out of the study.

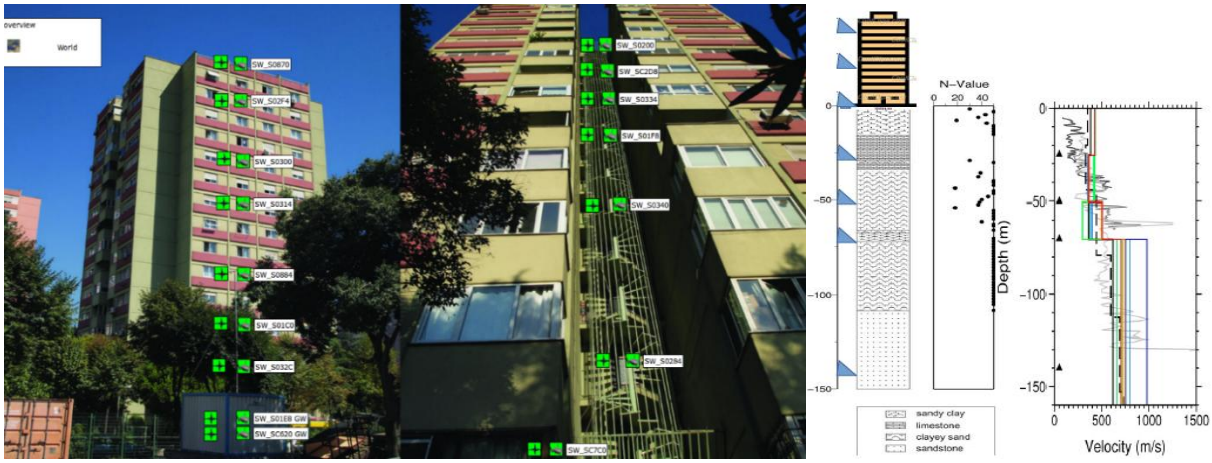

Figure 2. The B22 building and the container of the downhole array (left), SOSEWIN instrumental configuration (Left and center), and schema of Ataköy vertical array (downhole and building installation) and the velocity profile (right).

4 APPLICATION

4.1 DECONVOLUTION

An example of the application of the interferometric approach is shown in Fig. 3 for a M=4.4 earthquake that was recorded by the borehole installation in Gaziköy, consisting of a sensor at 0m and one at -143.6m. Both the surface station and the one at -143.6 m are used as reference stations. The shear wave velocities are estimated by calculating the time-lags between the propagation pulses at the surface and downhole, using the deconvolution with respect to the surface sensor and the downhole sensor. We estimate in this case only the average velocity in the borehole, since recordings from only two sensors are available. If more borehole sensors were installed at different depths, then the velocity of the layer between two sensors could be estimated. By stacking the results of more events, the accuracy of the results can be further improved.

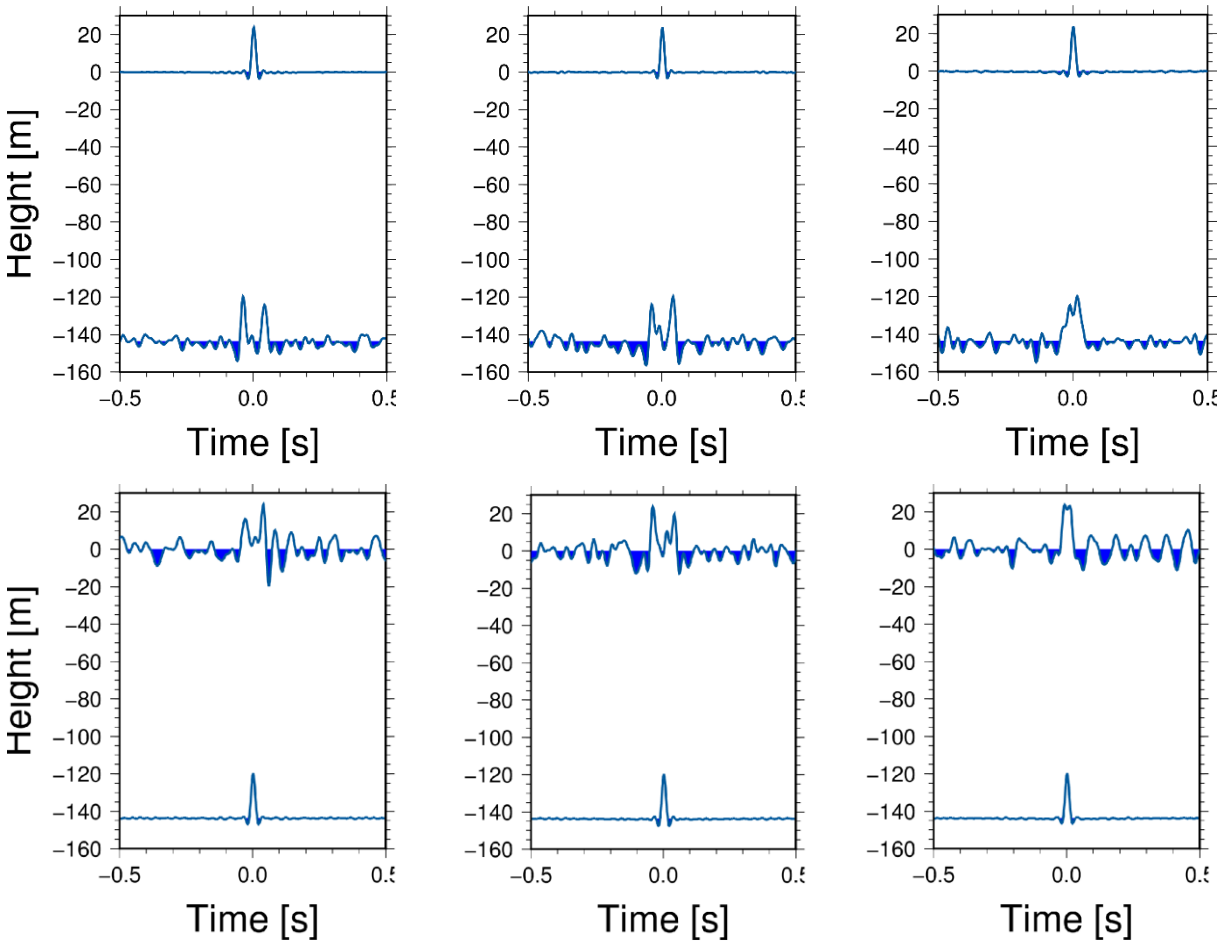

Figure 3. Deconvolved wavefield obtained after deconvolving the recordings at -143.6 m with the recordings at 0 m as the reference (top). Deconvolved wavefield obtained after deconvolving the recordings at 0 m with the recordings at -143.6 m as a reference (bottom). The recordings of the broadband seismometers at 0 m and -143.6 m depth of the 16.12.2014 (M=4.4) earthquake are used. Left: North-South, middle: East-West, right: Vertical component.

4.2 CONSTRAINED DECONVOLUTION

The constrained deconvolution approach (Bindi et al., 2010) is applied to the surface and downhole recordings of the borehole of the M=4.4 earthquake (deconvolution shown in Section 4.1) and presented in Fig. 4, top left panel. The peak of the down-going wave has almost the same amplitude as the upgoing wave, pointing to the fact that a large amount of energy is reflected back from the surface, indicating how removing the downgoing wave is an important issue. The input motion at the base of the borehole is computed, removing the down-going waves by the use of the obtained propagator (see Fig. 4). In the top right panel, the Fourier amplitude spectra of the surface recordings (red) and the downhole recordings (blue) are shown. It is worth mentioning that the input data are not converted yet to [m/s], but are still in counts. The correction for the instrumental response still has to be performed, which will lead to a change of scaling. The spectral ratio of these two Fourier

amplitude spectra (red), characterized by the presence of spectral troughs related to the negative interference generated by the downgoing wave, are presented, together with the spectrum of the constrained Landweber solution (black), in the bottom left panel. In the right bottom panel, the comparison between the downhole spectra and the input motion obtained by the constrained deconvolution are shown in the Fourier domain. The results obtained seem to indicate that the removal of the down-going wavefield from the input motion might lead to changes in the estimated source parameters due to the modification of the shape of the input spectra.

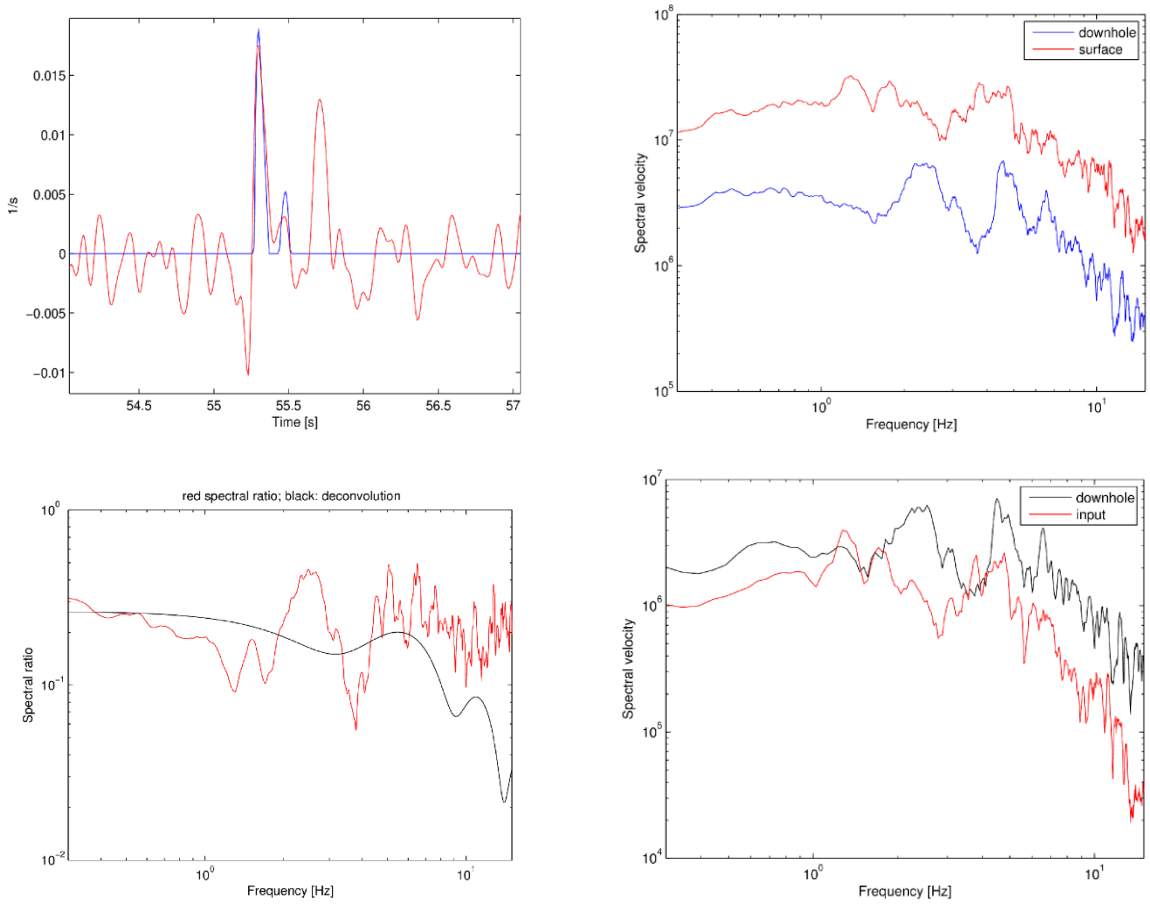

Figure 4. Constrained deconvolution analyses for the 16.12.2014 (M=4.4) earthquake recorded at the Gaziköy array. Top left: Results of the downhole-to-surface deconvolution, without any constraints (red) and the constrained solution (blue). Top right: Fourier spectra of the surface (red) and downhole recordings (blue). Bottom left: Spectral ratio between the downhole and surface recordings (red) and the constrained Landweber solution (black). Bottom right: Spectrum of downhole recording (blue) and the spectrum restored by deconvolution (red).

4.3 JOINT DECONVOLUTION

The data set that is used for the analysis of wave propagation through the building and soil consists of 5 earthquake recordings with magnitudes ranging from M=3.7-4.8 that mainly occurred in the Marmara Sea region (see Table 1). The recordings of event no. 4 (Table 1) are shown in Fig. 5 for the building and downhole sensors.
Fig. 6 shows the deconvolved wavefield obtained for one horizontal direction by applying the joint deconvolution approach (the sensors installed in the borehole are rotated to be aligned with the main axes of the building) and using the station installed at the roof of building B22 as a reference for the 5 events separately (left) and after stacking (right). In the acausal part of the deconvolved wavefield, a clear up-going wave can be identified that propagates from the downhole sensor at 140 m depth until the Earth‘s surface. Part of the energy is transmitted to the B22 building and propagated until the roof, the other part is reflected at the Earth‘s surface and propagates as a down-going wave. The waves that reach the roof of the building are completely reflected back, where again at the Earth‘s surface some of the energy is transmitted back to the soil and some reflected back into the building. The waves radiated back from the building to the soil are clearly visible until 50 m depth, but can be identified also at the sensor at -140 m.

The estimation of the wavefield radiated back to the soil is based on 1) detailed identification of the peaks of the deconvolved wavefield, 2) estimation of the real seismic input, and 3) estimation of the part of the wavefield describing the propagation from the building to the ground (Petrovic and Parolai, 2016).
Numerical simulations are performed using the approach of Wang (1999) to better understand the wave propagation through the building-soil structure and finally, to identify the peaks of the deconvolved wavefield. Different from the test case of a 3 storey masonry building as shown in Petrovic and Parolai (2016), the velocity of the B22 building is not homogenous, but decreases with the height of the building. The building is approximated as a shear beam, with three layers with the building’s velocity structure added to the top of the soil layers. To better understand the results, the deconvolved wavefield of the synthetic seismograms is compared with the results obtained after stacking of the deconcolved wavefield of the 5 analyzed earthquakes.
Since peaks associated with different wave phases arrive at the same time (see Petrovic and Parolai, 2016), the calculation of the analytical transfer function helps in the more detailed identification of the peaks. In the case of B22 as mentioned above, the velocity structure of the building can be described by three layers with different velocities. First, the part of the down-going wave reflected at the top of the building and propagated until the Earth’s surface has to be separated by considering a three layered model. Second, the down-going waves radiated back from the building to the soil (at 23m and 50m) are estimated by considering the lowermost layer of the building and the two uppermost layers of the soil (from 0m to 23m and from 23m to 50m).
The real seismic input (after removing all down-going waves reflected at the impedance contrasts) is estimated by application of the constrained deconvolution approach (Bindi et al., 2010). For this purpose the deconvolution interferometry is calculated by using the downhole sensor at 0m as the reference. The peak associated with the upward-propagating wave is isolated and after its convolution with the recordings at 0m, the real seismic input is obtained. The same approach is performed to calculate the wavefield radiated back from the building to the soil, using the recordings at the top of the building as the reference. In this case, the multiple arrivals of different phases at the same time has to be taken into account. For further details, see Petrovic and Parolai (2016).

Table 1. List of events used in this study.

Event ID	Date	Time	Location	Depth	Magnitude	Distance to epicenter
1	27.11.2013	04:13:37	40.85N, 27.92E	9 km	4.8	80 km
2	27.11.2013	04:21:35	40.85N, 27.91E	7 km	4.0	80 km
3	05.02.2014	01:56:44	41.36N, 28.61E	12 km	3.7	45 km
4	28.10.2015	16:20:03	40.80N, 27.72E	16 km	4.6	100km

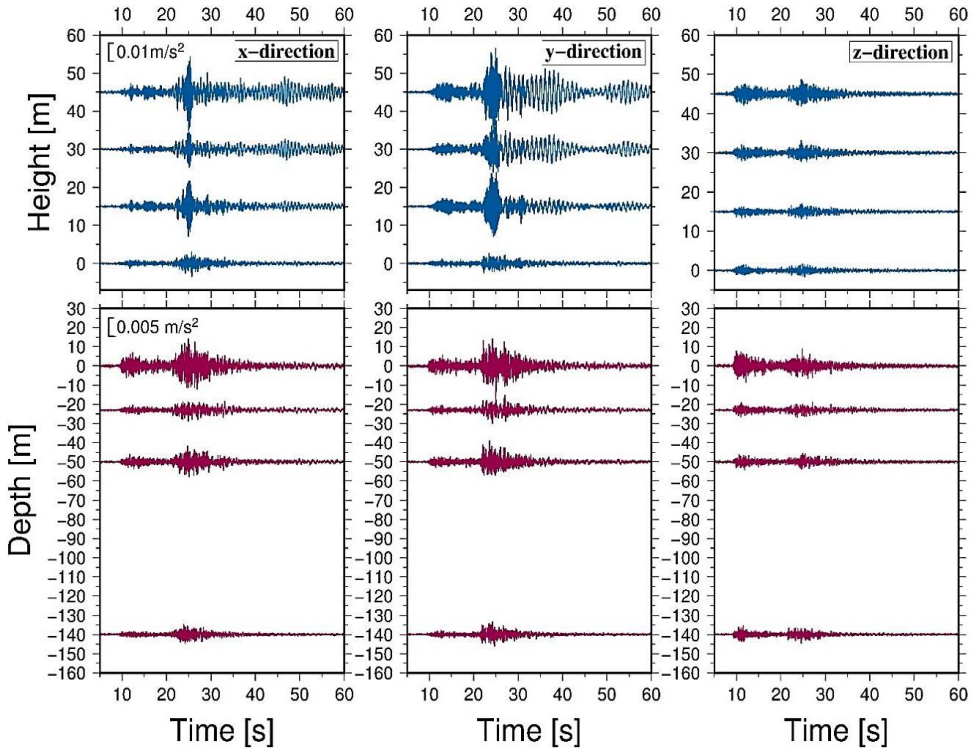

Figure 5. Recordings of event no. 4 (Table 1) of the building (blue) and the downhole sensors (violet).

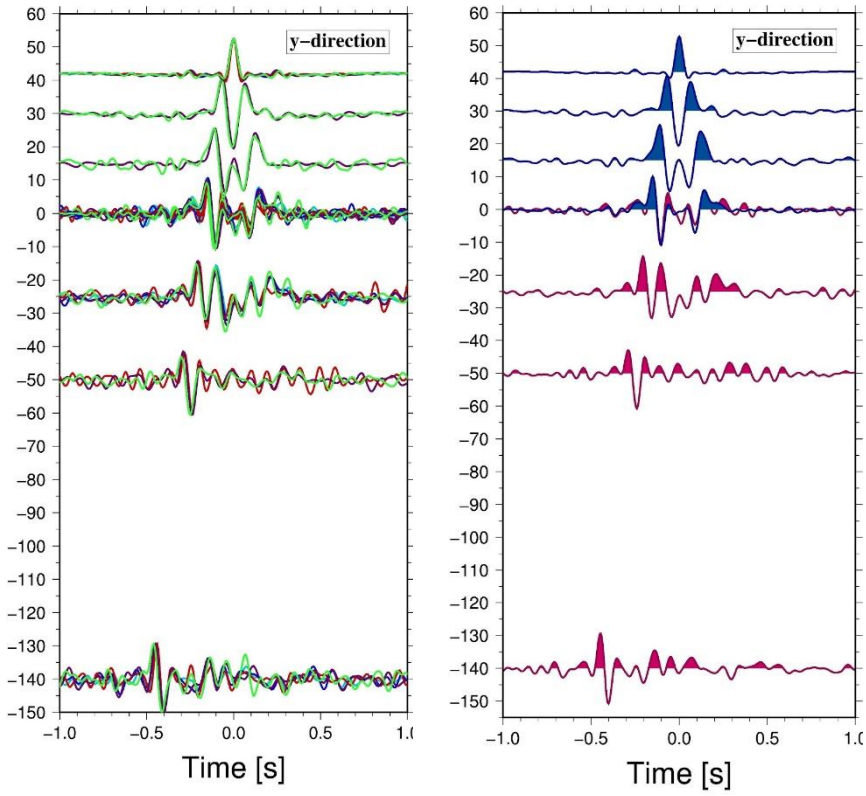

Figure 6. Left: Deconvolved wavefields using the station at the roof of the building (B22) as the reference for the 5 events listed in Table 1. Right: Results after stacking.

5 CONCLUSIONS

- Analysis of the wave propagation through the building, the soil or the building-soil structure, including transmitted waves and waves reflected at the different layers, the surface and the top of the building, was performed.
- Quantification of the amount of energy radiated back from the building to the soil even for complicated underground velocity structures and without a priori knowledge of velocity and quality factor Q is possible.
- Waves radiated back from the structure are not negligible.
- Possible interactions between nearby buildings should be considered.

6 References

Assimaki, D., Li, W. Steidl, J.H. & Tsuda, K., 2008. Site amplification and attenuation via downhole array seismogram inversion: a comparative study of the 2003 Miyagi-Oki aftershock sequence, *Bull. seism. Soc. Am.*, 98, 301–330.

Bindi, D., S. Parolai, M. Picozzi and A. Ansal (2010). Seismic input motion determined from a surface-downhole pair of sensors: a constrained deconvolution approach. *Bull. Seism. Soc. Am*., **100**, no. 3, 1375-1380.

Cheng, M. H., M. D. Kohler and T. H. Heaton (2015). Prediction of wave propagation in buildings using data from a single seismometer, Bull. Seism. Soc. Am., **105**, no. 1,107-119.

Dikmen, S.U., A. Edincliler, and A. Pinar (2015). Northern Aegean Earthquake (Mw=6.9): Observations at three seismic downhole arrays in Istanbul. *Soil Dyn. Earthq. Eng.*, Vol. 77, pp. 321-336.

Dikmen, S. U., A. Pinar, and A. Edincliler (2016). Near-surface attenuation using traffic-induced seismic noise at a downhole array, *J. Seismol.*, Vol. 20, pp. 375-384.

Mehta, K., R. Snieder, and V. Grazier (2007a). Extraction of near-surface properties for a lossy layered medium using the propagator matrix, *Geophys. J. Int*., **169**, 2171-280.

Mehta, K., R. Snieder and V. Grazier (2007b). Downhole receiver function: a case study, *Bull. Seism. Soc. Am.*, **97**, 1396-1403.

Nakata, N. and R. Snieder (2014). Monitoring a building using deconvolution interferometry. II: Ambient-vibration-analysis, *Bull. Seism. Soc. Am*., **104**, no. 1, 204-213.

Nakata, N., W. Tanaka, and Y. Oda (2015). Damage detection of a building caused by the 2011 Tohoku-Oki earthquake with seismic interferometry, *Bull. Seism. Soc. Am.*, **105**, no. 5, 2411-2419.

Nakata, N., R. Snieder, S. Kuroda, S. Ito, T. Aizawa, and T. Kunimi (2013). Monitoring a building using deconvolution interferometry. I: Earthquake-data analysis, *Bull. Seism. Soc. Am*., **103**, no. 3, 1662-1678.Newton, C. and R. Snieder (2012). Estimating Intrinsic Attenuation of a Building Using Deconvolution Interferometry and Time Reversal, *Bull. Seism. Soc. Am*., **102**, no. 5, 2200-2208.

Newton, C. and R. Snieder (2012). Estimating Intrinsic Attenuation of a Building Using Deconvolution Interferometry and Time Reversal, *Bull. Seism. Soc. Am*., **102**, no. 5, 2200-2208.

Oth, A., S. Parolai, D. Bindi (2011). Spectral analysis of K-NET and KiK-net data in Japan, Part I: Database compilation and peculiarities, *Bull. Seism. Soc. Am*., **101**, no. 2, 652-666.

Parolai, S., A. Ansal, A. Kurtulus, A. Strollo, R., Wang and J. Zschau (2009). The Ataköy vertical array (Turkey): insights into seismic wave propagation in the shallow-most crustal layers by waveform, *Geophys. J. Int.*, **178,** 1649-1662

Parolai, S., D. Bindi, A. Ansal, A. Kurtulus, A. Strollo and J. Zschau (2010). Determination of shallow S-wave attenuation by down-hole waveform deconvolution: a case study in Istanbul (Turkey), *Geophys. J. Int*., **181**, no. 2, 1147-1158.

Parolai, S. D. Bindi, S. Ullah, S. Orunbaev, S. Usupaev, B. Moldobekov, H. Echtler (2013). The Bishkek vertical array (BIVA): acquiring strong motion data in Kyrgyzstan and first results, *Journal of Seismology*, **17**, no 2, 707-719.

Parolai, S., R. Wang and D. Bindi (2012). Inversion of borehole weak motion records observed in Istanbul (Turkey), *Geophys. J. Int*., **188,** no 2, 535-548.

Petrovic, B. and Parolai, S. (2016) Joint deconvolution of building and downhole strong motion recordings: Evidence for the seismic wavefield being radiated back into the shallow geological layers, *Bull. Seism. Soc. Am.*, in press

Picozzi, M., S. Parolai, M. Mucciarelli, C. Milkereit, D. Bindi, R. Ditommaso, M. Vona, M..R. Gallipoli and J. Zschau (2009). Interferometric Analysis of Strong Ground Motion for Structural Health Monitoring: The Example of the L'Aquila, Italy, Seismic Sequence of 2009, *Bull. Seism. Soc. Am*., **101**, no. 2, 635-651.

Rahmani, M. and M. I. Todorovska (2013). 1D system identification of buildings during earthquakes by seismic interferometry with waveform inversion of impulse responses – method and application to Millikan library, *Soil Dyn. Earthq. Eng., **47**, 157–174.*

Snieder, R. and E. Şafak (2006). Extracting the building response using seismic interferometry: Theory and application to the Millikan library in Pasadena, California, *Bull. Seism. Soc. Am*., **96**, 586-598.